

# An experimental study on hybrid fibre reinforced engineered cementitious composite link slabs under static and fatigue loadings

Shiyao Zhu<sup>a</sup>, Y.X. Zhang<sup>b</sup>, C.K. Lee<sup>a,\*</sup>

<sup>a</sup> School of Engineering and Technology, University of New South Wales, Canberra, ACT 2600, Australia

<sup>b</sup> School of Engineering, Design and Built Environment, Western Sydney University, Kingswood, NSW 2751, Australia

## ARTICLE INFO

### Keywords:

Engineered cementitious composite (ECC)  
Hybrid fibres  
Link slab  
Fatigue test  
Crack width control

## ABSTRACT

This study conducted experimental investigations on the structural performances of link slabs which are constructed by using a newly developed hybrid-fibre reinforced engineered cementitious composite (hybrid-ECC). Both static and fatigue loadings were applied to validate the feasibility, provide a proof of concept study and demonstrate the benefits using hybrid-ECC for bridge link slabs application. Three identical quarter-scaled hybrid-ECC link slabs, simulating a link slab used for a typical 35-meter multi-span simply supported bridge, were fabricated. These slabs, denoted as LS-1, LS-2 and LS-3, were tested under designated static and fatigue loadings. Slab LS-1 was tested under static loading to obtain the flexural strength of the slab. Slabs LS-2 and LS-3 were tested under fatigue loadings to evaluate their fatigue performances under normal service loading and overload scenarios, respectively. Structural performances of these slabs in terms of deformation and crack width control capability, strain development on reinforcement bars and estimated service life were evaluated. It was observed that multiple microcracks were developed under both static and fatigue loadings. Slab LS-2 survived ten million cycles of service fatigue loading while LS-3 survived two million cycles of overload fatigue loading. For all the tests conducted under static and fatigue loadings, the maximum crack width observed on the three link slab samples was all controlled within the allowable limit of 0.2 mm until failure occurred. Based on the test results, it was estimated that if only the effects due to normal traffic loading and temperature variation were considered, the hybrid-ECC link slab could achieve a service life of more than 40 years. Therefore, the experimental study reconfirmed that the hybrid-ECC showed a high potential to improve the fatigue performance and extend the service life of link slab in bridge construction.

## 1. Introduction

Engineered cementitious composite (ECC) is a kind of cementitious composite reinforced by employing short fibres, such as polyvinyl alcohol (PVA) fibres, polyethylene (PE) fibres and steel fibres [1]. Many types of ECCs have been developed and they demonstrated different material properties when different fibres are used. For example, while steel fibre reinforced ECC was found to show a relatively high tensile strength of 7–16 MPa, its ultimate strain was relatively low of around 0.5% [2–4]. On the other hand, polyethylene fibre reinforced ECCs demonstrated a high ultimate tensile strain of 3%–9% [2,4,5] but a relatively low tensile strength of less than 7 MPa. Furthermore, it was found that ECCs' material properties were tailorable by employing different fibres at different volume fractions. Many types of hybrid fibre reinforced ECCs (hybrid-ECCs) which contain both polymer and steel

fibres were developed with a balanced performance in terms of strength and strain capability [3,6]. Link slabs were commonly used to fill up the expansion joint in simply supported girders as well as transverse joints between tub girders in a continuous bridge [7,8]. Therefore, construction of link slabs required the use of suitable building materials with good deformation ability, strength capacity and crack width control ability. However, concrete material is brittle in nature and has limited tensile strength and insufficient crack width control ability for link slab application. Towards this end, a new type of hybrid-ECC with 1.25% PE fibre and 0.75% steel fibre in volume fractions was specially developed by Zhu et al. [6] for link slab application to achieve strength and strain capability which are both critical performance factors. In addition, Zhu et al. [6] also simplified and translated the structure performance requirements into a set of material properties requirements based on the section design method. However, in [6], no detailed experimental

\* Corresponding author.

E-mail address: [chi.k.lee@unsw.edu.au](mailto:chi.k.lee@unsw.edu.au) (C.K. Lee).

<https://doi.org/10.1016/j.engstruct.2023.117254>

Received 4 January 2023; Received in revised form 16 November 2023; Accepted 26 November 2023

Available online 2 December 2023

0141-0296/© 2023 The Author(s). Published by Elsevier Ltd. This is an open access article under the CC BY license (<http://creativecommons.org/licenses/by/4.0/>).

studies on link slabs fabricated by using the developed ECCs was conducted to evaluate and confirm the actual performance of the ECC developed at structural level application.

Caner and Zia [8] investigated the structural behaviour of a concrete link slab and suggested its feasibility for practical applications. However, concrete link slab was found to exhibit cracks under normal service load. For example, a maximum crack width of 0.25 mm was observed at 37% of the ultimate strength of the concrete link slab and it was increased to 0.61 mm at 78% of the ultimate strength. These values were greater than the maximum allowable crack width limits of 0.2 mm for aggressive environmental conditions prescribed by the VicRoads code [9].

In some previous studies [8,10–13], researchers investigated the structural performances as well as the crack width development history of link slabs under fatigue loading, and ECC link slabs were found to show a better crack width control ability. Kim et al. [10] found that after one hundred thousand cycles of service loading, crack width in their ECC link slab was less than 0.05 mm while the crack width of a similar concrete link slab crack was 0.64 mm. Hou et al. [11] demonstrated that ultra-high ductile ECC link slabs survived two million fatigue load cycles while an average crack width of 0.05 mm was observed. It was noted that due to time limitation, Hou et al. [11] only applied two million cycles in their test which was equivalent to just a 2-year service period of equivalent single axle load (ESAL) [14]. Although some other experimental studies on the ECC link slabs under designed fatigue loadings were conducted [10,11], again due to the insufficient numbers of fatigue load cycles applied, their service life under actual service conditions could not be estimated. In order to understand the long-term fatigue behaviours of ECC link slabs under service loading condition, fatigue tests involving up to ten million load cycles are required.

In addition, due to resource limitations, many tests conducted were based on scaled models of an actual link slab. For instance, a 1/3 scaled concrete link slab was prepared by Au et al. [15] while a small scale monofibre ECC link slab of 810 mm long was tested by Chu et al. [16]. Although some investigations were conducted to optimise the design of link slab in terms of the debonding length and supports conditions [12, 13], there was no standard to follow for designing a scaled model. In this work, a detailed process of design of scaled link slab was developed, which would be valuable and beneficial to the future investigation of the scaling effects between laboratory test and field test.

This work presented an experimental study on the structural performance of hybrid-ECC link slabs under both static and fatigue loadings. Three quarter-scaled link slab was prepared to simulate a full link slab applied on a simply supported bridge with 35 m span. The hybrid-ECC with 1.25% PE fibre and 0.75% steel fibre developed by the authors [6] was employed. These three link slabs, namely LS-1, LS-2 and LS-3 were fabricated with the same material in identical geometry. Link slab LS-1 was tested under static loading in order to obtain the flexural strength and the crack control capability of ECC link slab under static loading condition. LS-2 was tested under service fatigue loading up to ten million cycles to evaluate its performance under real life service scenario. LS-3 was first subjected to two million overload fatigue cycles and then followed by a static test until failure so that both the damage behaviours and residential strength of the slab could be studied. Test results from LS-2 and LS-3 would also allow the service life of the slabs to be estimated. During all tests, key performances of these three slabs, including ultimate strength capacity, deformation capacity, strain development on ECC surface and reinforcement bars and cracking behaviour were investigated so that the feasibility of using hybrid-ECC link slab in practical bridge construction could be evaluated.

## 2. Experimental program

### 2.1. Design of the quarter-scaled link slabs

The quarter-scaled link slabs tested in this study was designed to

investigate their structural behaviour under static and fatigue loadings induced by both traffic loading and temperature variation. Fig. 1 shows the general layout of two girders connected by a link slab and the interested region which is the focus of the experimental study. As shown in Fig. 1a and Fig. 1b, the length of the specimen was determined by the length of the link slab and the length between the zero moment positions (i.e., inflection points) of the main girders under design load. By introducing the inflection point, the two full span girders could be simplified into two portions supported by a pin and a roller [10] for the laboratory test. The length between the inflection points  $L_{Test}$  can be calculated by Eq. 1.

$$L_{Test} = \text{inflection point ratio} \times \sum_{i=1,2} L_{girder,i} \quad (1)$$

In Eq. 1,  $L_{girder,i}$ ,  $i = 1,2$  is the length of the effective span of the  $i^{th}$  girder. The inflection point ratio was suggested to be between 6% and 7% for a simply supported bridge [10,17]. In this study, a value of 7% was adopted.

As shown in Fig. 1c, a link slab has one debonding zone in the middle and two bonded zones at the two ends. The bonded zone transfers the deformation from the girders via shear studs and interfacial bonding between the girders and link slab surfaces. The debonding zone minimises local tensile strain and stress concentration within the connection region. It also prevents the formation of kink within the link slab [13,14, 18]. The total length of the link slab  $L_{ls}$  can be calculated by using the length ratio and length of the girders [18] as shown in Eqs. 2–4.

$$L_{ls} = \sum_{i=1,2} L_{bond,i} + L_{de} \quad (2)$$

$$L_{bond,i} = \text{bond length ratio} \times L_{girder,i} \quad (3)$$

$$L_{de} = \text{debond length ratio} \times \sum_{i=1,2} L_{girder,i} \quad (4)$$

In Eqs. (2) to (4),  $L_{ls}$ ,  $L_{bond,i}$  and  $L_{de}$  is the total length, the bond length and the debonding length of the link slab, respectively. From the parametric studies conducted in [12,13,19], a bond length ratio of 2.5% and a debonding length ratio of 5% of adjacent span lengths were recommended for general link slab design.

In this study, due to limitation of space and equipment capacity, a quarter-scaled model was adopted to investigate the structural performance of a link slab designed for a simply supported bridge with 35 m span length [20]. Table 1 summarises the scaling design process (Step I to Step IV) and calculation results. Firstly, in Step I, details of a full-scale bridge were determined. In this step, the full span length  $L_{girder}$ , bearings positions from the girder end  $L_{bearings}$  and the gap between girders' ends  $L_{gap}$  were retrieved from standard design drawings of a full-scale bridge. Based on these data, the length within the inflection points  $L_{Test}$  was determined by Eq. 1 in Step II. After that, the design length of the link slab  $L_{ls}$  was calculated by Eqs. 2–4 where the debonding length  $L_{de}$  and bonded length  $L_{bond}$  were calculated in Step III. Finally, scale factor was then applied in Step IV to calculate the scaled lengths  $L'_{Test}$ ,  $L'_{bond}$ ,  $L'_{de}$ , and  $L'_{bearings}$  of the scaled link slab. As shown in Fig. 1, for simplification, scaling was only applied to the length of the bridge. The dimensions of the quarter-scaled model were given in Table 1. It should be noted that dimension of  $L'_{bearings}$  was rounded to the nearest 50 mm. A gap length  $L'_{gap} = 45$  mm was adopted to ensure that there is enough space for the movement of the top ends of the steel girder during the test.

### 2.2. Preparation of specimens and tests setup

All test specimens were prepared in the same way using a reusable mould. As shown in Fig. 2a, a wooden mould was placed at the bottom part of the casting setup. The steel reinforcement bars were placed in the mould before casting. Spacers were properly used to ensure steel reinforcement bars were correctly placed at desired locations when casting.

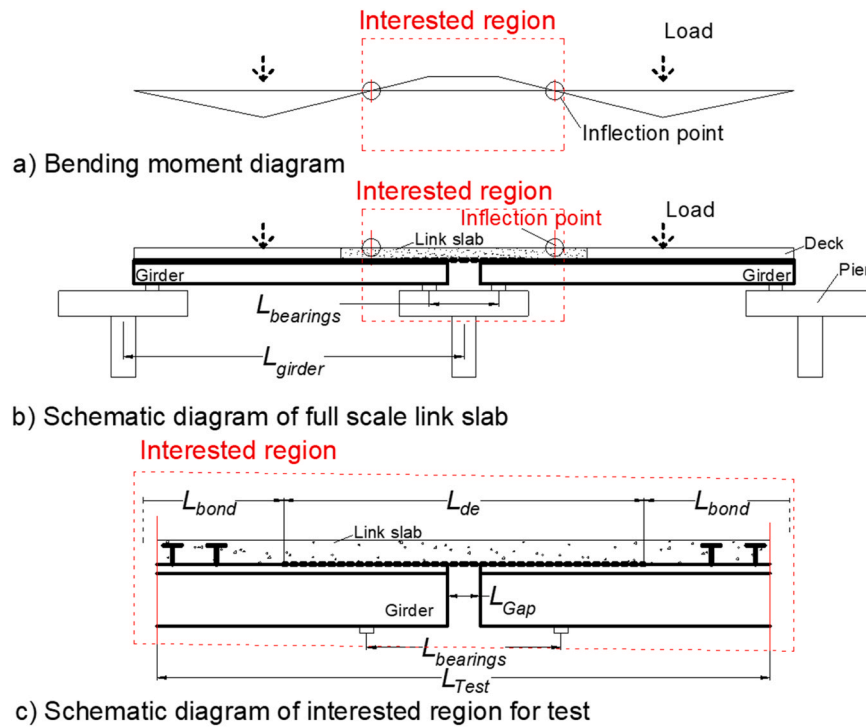


Fig. 1. Typical link slab design for a simply supported beam bridge.

Table 1

Geometry parameters of the quarter scaled link slab.

STEPS	Calculations and derived values
Step I	$L_{girder,1} = L_{girder,2} = 35000$ mm; $L_{bearings} = 950$ mm; $L_{gap} = 50$ mm
Step II	Defining inflection point ratio= 7%, by Eq. 1 $L_{Test} = 4900$ mm;
Step III	Defining bond, debonding length ratio= 2.5%, 5% respectively, by Eqs. 2 - 4 $L_{bond,1} = L_{bond,2} = 875$ mm, $L_{de} = 3500$ mm; $L_s = 7000$ mm
Step IV	Defining scale factor= 0.25 $L'_{Test} = 1275$ mm; $L'_{bond,1} = L'_{bond,2} = 219$ mm; $L'_{de} = 875$ mm; $L'_{bearings} = 250$ mm

Two steel beams were temporarily connected by bolts and supported by the mould. After the mould setup was ready, the ready-mixed hybrid-ECC was smoothly cast into the mould. Vibration was applied carefully to ensure the casting quality. After one day, the link slabs were demoulded and moved to a fog room for standard curing conditions where the temperature was kept at  $23 \pm 2$  °C and relative humidity at  $95 \pm 5\%$  for 28 days until testing.

During the static and fatigue tests, as shown in Fig. 2b, the link slab was tested invertedly to simulate the bending effects under design traffic loading and temperature variation. The pin and roller supports were set at the inflection points. The distance between the supports was  $L'_{Test} = 1275$  mm. The loading points simulated the inverted bearing supports on the pier and the distance between two supports was  $L'_{bearings} = 250$  mm. As shown in Fig. 2, two roller supports were adopted to simulate the most commonly used support conditions of expansion bearings, which allows rotational and longitudinal movements. A gap length  $L'_{gap} = 45$  mm was adopted to ensure there is enough space for the beam to deform during the test. The ECC link slab was connected to two 150UC steel beams as support girders by shear studs at both ends. The selected 150UC beam has a flexural stiffness nearly seven times that of the ECC slab so it would provide sufficient stiffness for the load/deformation transmission. As shown in Fig. 2c, six shear studs were arranged in two rows at the end of each steel beam with a spacing of 100 mm in both horizontal and longitudinal directions. Each shear stud has a shank

diameter of 13 mm and a shank length of 50 mm. The stud head measures 25 mm in diameter and 7 mm in height. The length, width and thickness of the ECC link slab is 1525 mm, 300 mm and 100 mm, respectively. The slab has a 125 mm extended span out of the supports at both ends. Plastic sheets were placed between the steel beams and slab to form a debonding length of 875 mm. In order to provide a consistent and stable debonding interface between the steel beams and the hybrid-ECC slab, UV stabilised polypropylene sheets with a thickness of 150  $\mu$ m were used in all test specimens. The polypropylene sheet provides negligible frictional coefficient between the steel and hybrid-ECC interface and therefore generated negligible bond strength between the steel beams and the hybrid-ECC slab at the debonding region. The plastic sheets were placed at the end of each steel beam before casting, while excess parts (indicated in Fig. 2a) were cut off before testing (see Fig. 2b). Three  $\text{\O}12$  mm D500N deformed reinforcement bars with elastic modulus of 200 GPa and yield strength of 500 MPa (yield strain is 2500  $\mu$  $\epsilon$ ) were placed within the ECC slabs to achieve a reinforcement ratio of 1.13% as suggested in previous designs [10,11]. The length of reinforcement bars embedded in the transition zone is 375 mm (see Fig. 2c), which is sufficient for reinforcement bars to develop strength during the test. The hybrid-ECC with 1.25% PE fibre and 0.75% steel fibre developed by Zhu et al. [6] was used for the fabrication of the link slabs. The mix design of the ECC given in Table 2. The ECC's material properties obtained from standard compressive [21] and tensile tests [22,23] are given in Table 3. The strain capacity of the hybrid-ECC was 2.7%, which met the requirement to accommodate the induced strains and longitudinal deformation of the link slab caused by the live load and overall temperature effects [6].

Three link slabs, namely LS-1, LS-2, and LS-3 were fabricated with identical dimensions. LS-1 was tested under static loading to obtain its static failure strength. LS-2 and LS-3 were tested under fatigue loading to investigate their fatigue performances under service and overload scenarios, respectively. Please be noted that the relationship between the end rotation  $\theta_{end}$  and applied load, which was obtained from LS-1 static test, was used to determine the value of fatigue load that was applied to link slab LS-2 and LS-3. The loading schemes adopted were summarised in Table 4. For LS-2, fatigue test was conducted in two phases. In Phase I,

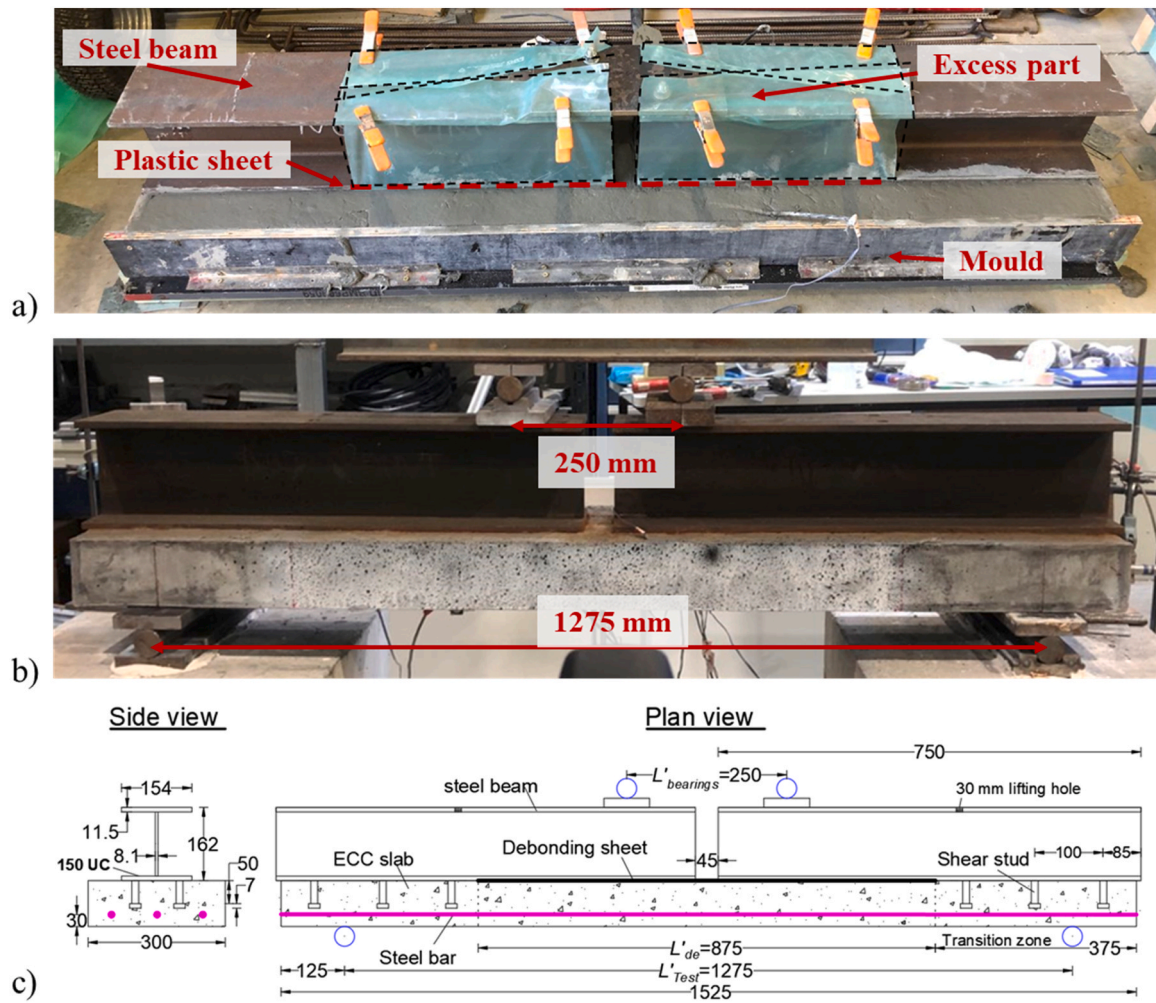


Fig. 2. Diagrams of a) casting setup, b) testing setup, and c) geometry parameters of the quarter-scaled link slab.

Table 2  
Mix design of hybrid-ECC.

Binder			Local Sand	Water	HRWR	PE	ST
GPC	SF	FA					
Ratio to Binder (w%)			Volume fraction (vol%)				
0.58	0.1	0.32	0.4	0.24	0.008	1.25	0.75

Legend: GPC = General Purpose Cement, SF=Silica Fume, FA=Fly Ash, HRWR=High Range Water Reducer (Superplasticizer), PE=Polyethylene fibre, ST=steel fibre

Table 3  
Material properties of hybrid-ECC.

Young's Modulus (GPa)	28.3
Tensile strength (MPa)	7.3
Strain at tensile strength (%)	2.7
Compressive strength (MPa)	94.5
Compressive strain (%)	0.46

ten million load cycles were applied with maximum and minimum load of 7.1 kN and 0.7 kN, respectively. The minimum load applied was set as 10% of the maximum load to ensure no sliding occurred during unloading. The maximum load was determined based on an end rotation of  $\theta_{end} = \theta_{field} = 0.001$  rad which is the maximum end rotation induced by traffic loading and temperature effect according to long-term field measurement during the service period [18,24]. After Phase I test was

Table 4  
Loading schemes for static and fatigue tests.

Specimens	Loading	lower	upper	load control method
		load /kN	load /kN	
LS-1	Static	-	-	displacement control, 0.5 mm/min
LS-2	Fatigue Phase I ten million cycles	0.7	7.1	force control, 4 Hz
	Fatigue Phase II (until failure)	5.1	50.8	force control, 1 Hz
LS-3	Fatigue two million cycles	3.4	33.6	force control, 1 Hz
	Static until failure	-	-	displacement control, 0.5 mm/min

completed, a higher loading range of 5.1–50.8 kN was applied in Phase II until fatigue failure. The link slab was considered to fail under fatigue load when the crack width limit of 0.2 mm was exceeded or the failure of reinforcement bars was observed, whichever comes first. The maximum applied load in Phase II was approximately corresponding to an end rotation  $\theta_{end} = 3 \times \theta_{allow} \approx 0.0113$  rad where  $\theta_{allow} = 0.00375$  rad is the maximum allowable rotation at the service limit state according to AASHTO [25]. Note that as rotation is dimensionless, both  $\theta_{field} = 0.001$  rad and  $\theta_{allow} = 0.00375$  rad are applicable to both full scale and scaled slabs.

For LS-3, in order to investigate its behaviour under an overload scenario, the minimum load and maximum load applied was set equal to

3.4 kN and 33.6 kN, respectively. The maximum load was corresponding to an end rotation  $\theta_{end} = 2 \times \theta_{allow} = 0.0075$  rad. LS-3 was first tested for two million load cycles. After that, static test would then be conducted to obtain the slab's residual strength.

Sinusoidal load was applied at a frequency of 4 Hz on LS-2 during Phase I test while a lower frequency of 1 Hz was applied in Phase II on LS-2 and on LS-3 as larger deformations would be developed under higher applied loads. As shown in Fig. 3, in all tests, the midspan deflection of the slab and the total crack mouth opening displacement (TCMOD), which is equivalent to the total lateral deformation of the midspan section measured along the length of the link slab, were monitored by two Linear Variable Differential Transformer (LVDT) LVDT-1 and LVDT-2, respectively. End rotations of the steel beams were recorded by LVDT-3 and LVDT-4. Strains of the reinforcement bars were monitored by six strain gauges S1-S6 while the strains at the ECC slab surface were monitored by other six strain gauges C1-C6. Digital image correlation (DIC) technic was also employed to monitor the crack development within the ECC by using a high definition DSLR camera taking plan view images of the centre part of the slabs during both static and fatigue tests.

### 3. Test results of LS-1

#### 3.1. load – deformation relationship

The load to midspan deflection curve of LS-1 is shown in Fig. 4. LS-1 showed a superior ductility under static loading. As shown in Fig. 4, LS-1 achieved its ultimate load capacity of 67.1 kN at a midspan deflection of 21.1 mm. This corresponded to a deflection-to-span ratio of 1/60. At the ultimate load, an end rotation of  $\theta_{peak} = 0.035$  rad was developed, which is almost 10 times of the allowable end rotation  $\theta_{allow} = 0.00375$  rad at

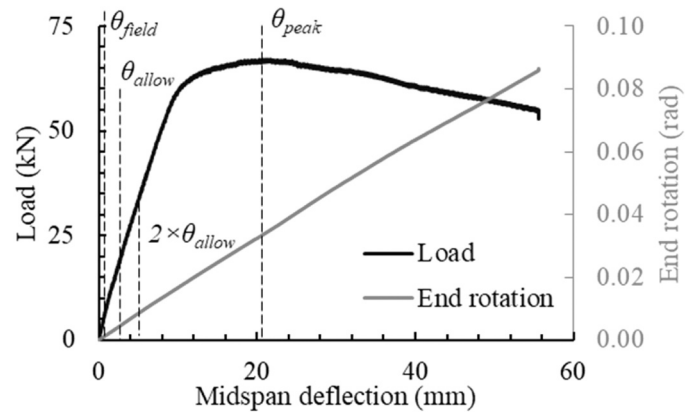


Fig. 4. Load to midspan deflection relationship under static loading for LS-1.

the serviceability limit state [25]. According to the pervious long-term monitoring that considered both traffic and temperature effects during the service period [18,24], the average field end rotation  $\theta_{field}$  was usually less than  $\theta_{allow}$  and is normally less than 0.001 rad. From Fig. 4., when the end rotation  $\theta_{end}$  is equal to 0.001 rad, the corresponding sustained load was 7.0 kN (11% of ultimate load capacity). Hence, this result suggested that the slab successfully accommodated the induced deformation at a low load level of 11% of the ultimate load capacity. In addition, when  $\theta_{end} = \theta_{allow} = 0.00375$  rad, the midspan deflection was 2.2 mm and the applied load was 17.8 kN (27% of its ultimate load capacity). Furthermore, when  $\theta_{end} = 2 \times \theta_{allow} = 0.0075$  rad, the sustained load was 33.6 kN (50% of ultimate load capacity) at a midspan deflection of 5.2 mm. It should be noted that at the ultimate load, cracks were observed in the slab, which eventually led to the link slab's failure.

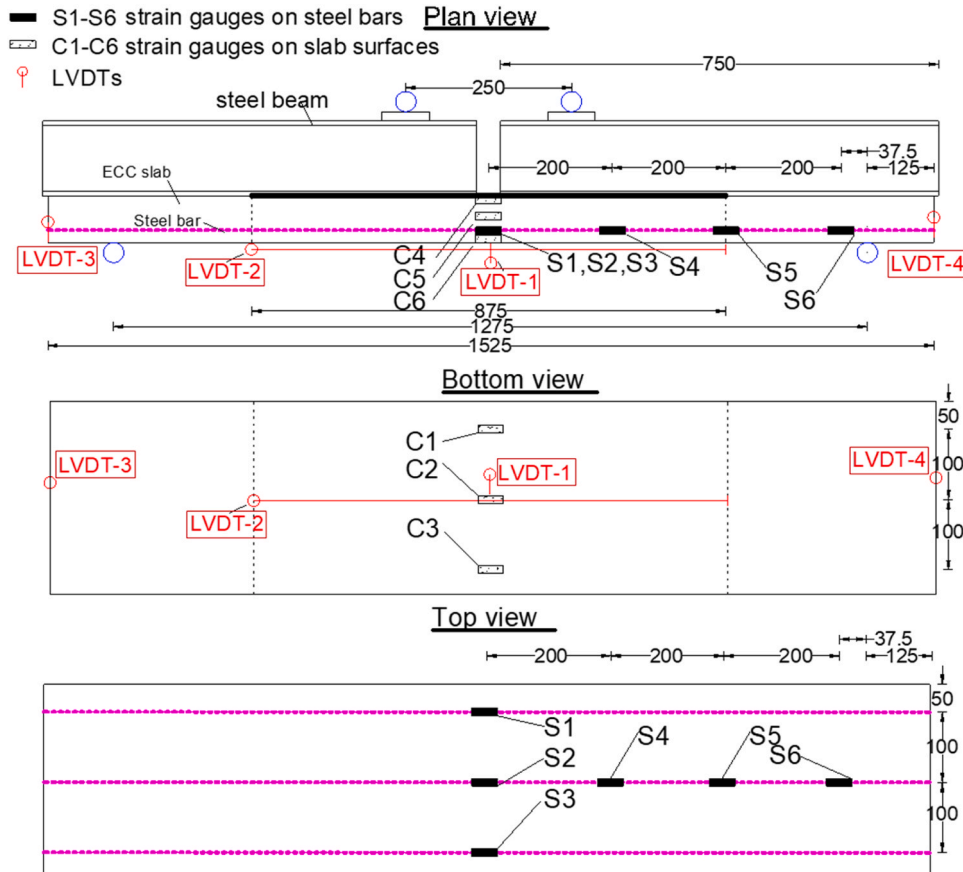


Fig. 3. Arrangement of LVDTs and strain gauges on steel bars (S1-S6) and slab (C1-C6).

Meanwhile, no slip was observed at the end of the steel reinforcement bars. No damages were observed at the shear stud connection area in the transition zone.

### 3.2. Cracking behaviour

Multiple cracking pattern of LS-1 under static loading captured by using DIC analysis was shown in Fig. 5. Fig. 5 also shows the development of the cracks as the end rotation was increased. As shown in Fig. 5a, no visible crack was observed when  $\theta_{end} = \theta_{field} = 0.001$  rad. At  $\theta_{end} = \theta_{allow} = 0.00375$  rad, a few microcracks could be observed (Fig. 5b). This demonstrated the promising crack control ability of the hybrid-ECC link slab under service limit state. More microcracks were observed at  $\theta_{end} = 0.0075$  rad (Fig. 5c) and a major crack was observed at the peak load as shown in Fig. 5d.

Fig. 6 shows that the maximum crack width was controlled within 0.144 mm until the ultimate load capacity. It should be noted that the maximum allowable crack width ( $w_{limit}$ ) for normal environmental condition was 0.3 mm according to VicRoads code [9]. However, a more stringent limit of  $w_{limit} = 0.2$  mm for aggressive condition was adopted here for evaluating the slab's performance [9]. After passing the ultimate load capacity, the major crack was widened and eventually led to the failure of the link slab. Fig. 7 shows the relationship between the TCMOD and midspan deflection. It shows that when the ultimate load capacity was reached, a TCMOD of 8.7 mm was observed. LS-1 accommodated a longitudinal deformation of 8.7 mm while the maximum crack width was controlled within the stringent crack width limit of

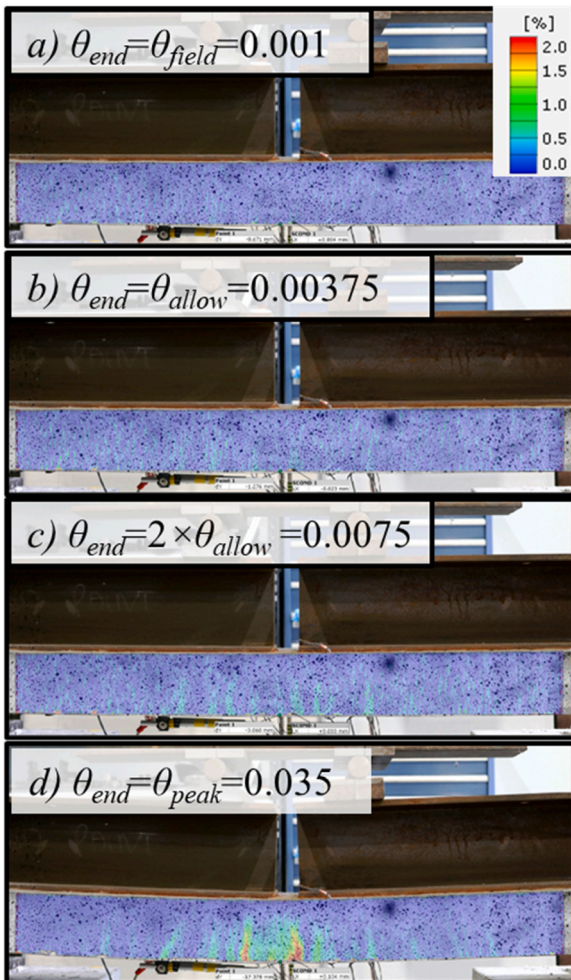


Fig. 5. Cracking behaviour under static loading.

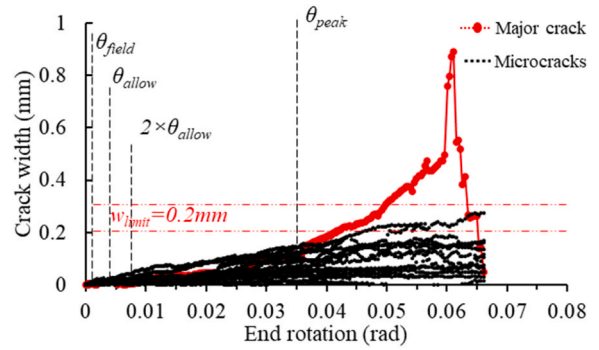


Fig. 6. Crack width development under static loading.

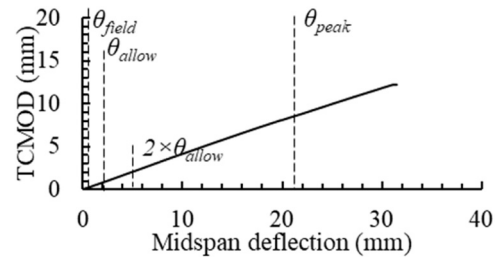


Fig. 7. Total crack mouth opening displacement (TCMOD) under static loading.

$w_{limit} = 0.2$  mm. These results demonstrated the advanced crack width control ability of the hybrid-ECC used.

### 3.3. Strain development in ECC and reinforcement bars

As shown in Fig. 8a, at the peak load ( $\theta_{end} = 0.035$  rad), the maximum tensile strain in the ECC slab was  $43972 \mu\epsilon$  which was recorded by gauge

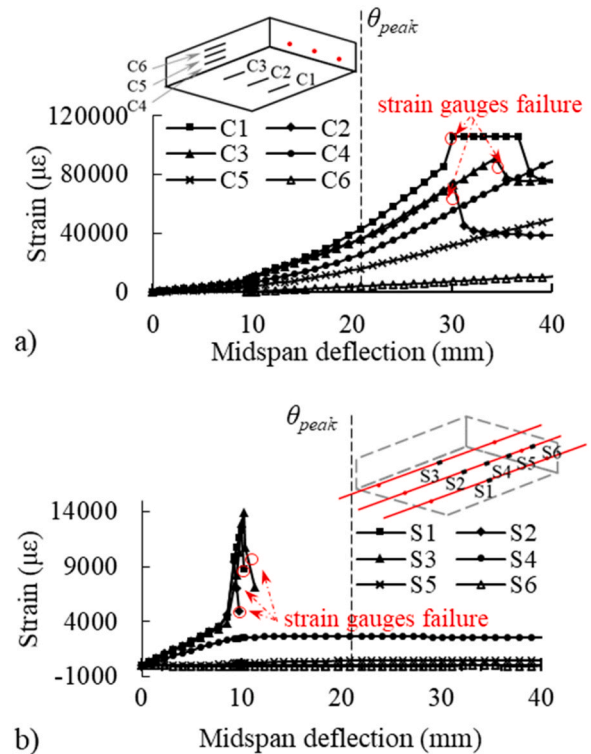


Fig. 8. Development of strains in LS-1 under static loading. (a) slab surfaces (C1-C6) and (b) reinforcement bars (S1-S6).

C1. It was found that the strain recorded by gauge C4 was lower than that by C1, C2 and C3. However, it continued to increase at later stage of the test. The delayed development of strain at C4 indicated the growing of cracks along the depth of the slab. For the reinforcement bars strains shown in Fig. 8b, higher strain was recorded at the midspan section by gauges S1, S2, and S3. It should be noted that some strain gauges were failed near the end of the test due to debonding with the measurement surfaces. In particular, strain gauges S1-S3 were failed when the midspan deflection reached 10 mm ( $\theta_{end}=0.016$  rad) while gauges C1, C2, C3 and C4 were failed after the midspan deflection exceeded 30 mm ( $\theta_{end}=0.049$  rad).

Fig. 9. shows the strain distribution as deformation increased. All measured strains were within the elastic limit of  $2500 \mu\epsilon$  until  $\theta_{end}=2 \times \theta_{allow}=0.0075$  rad. This showed that the hybrid ECC slab successfully limited the strain in the reinforcement bars even the end rotation well exceeded the allowable service limit. As expected, strains at different sections were in the order of  $S2 > S4 > S5 > S6$ . As shown in Fig. 9, the plastic strains mainly developed in sections S2 and S4 after  $\theta_{end}=2 \times \theta_{allow}=0.0075$  rad, which were within 200 mm away from the midspan section. For example, at the peak load ( $\theta_{end}=0.035$  rad), the strain at S4 section (200 mm away from the midspan) was  $2677 \mu\epsilon$ . Strain in reinforcement bar was decreased to  $447 \mu\epsilon$  at S5 section (400 mm away from the midspan section).

#### 4. Test results of LS-2 and LS-3

##### 4.1. Fatigue cycles and estimated service life

LS-2 survived the Phase I test of ten million cycles with a load range of 0.7–7 kN which was corresponding to a service loading with the maximum end rotation of  $\theta_{end} = \theta_{field} = 0.001$  rad [18,24]. After Phase I test was completed, LS-2 sustained a further 45,318 higher load range cycles (5.1–50.8 kN) in Phase II test before fatigue failure occurred. For LS-3, it survived two million cycles with a load range of 3.4–33.6 kN which was corresponding to an overload scenario with the maximum end rotation  $\theta_{end} = 2 \times \theta_{allow} = 0.0075$  rad. After the fatigue test, static loading was applied until the slab failed with a major crack developed and a residual strength of 67.5 kN.

Fig. 10 shows the estimated Equivalent Single Axle Load (ESAL) over years based on the annual traffic report in Australia [26]. A standard 80 kN ESAL and Load Equivalent Factor (LEF) of 1.7 ESALs/truck was used as default according to AASHTO design code [25]. According to the annual traffic report [26], the annual average daily traffic (AADT) of 16,000 vehicles with a truck percentage of 16% under an annual growth rate of 5% was used to estimate the ESALs over years.

The loads applied during the fatigue tests were converted to ESALs to estimate the corresponding service life. For Phase I test on LS-1 where

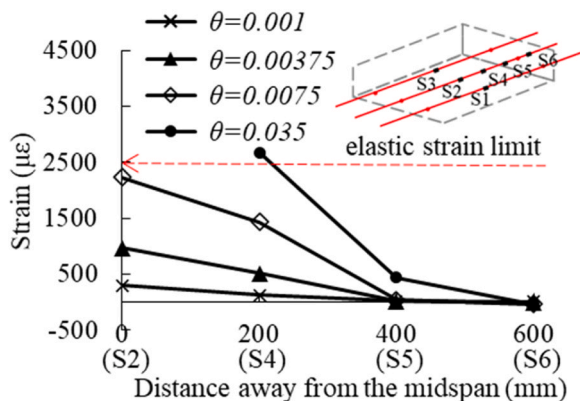


Fig. 9. Strain distribution along the steel bar with increased end rotations under static loading.

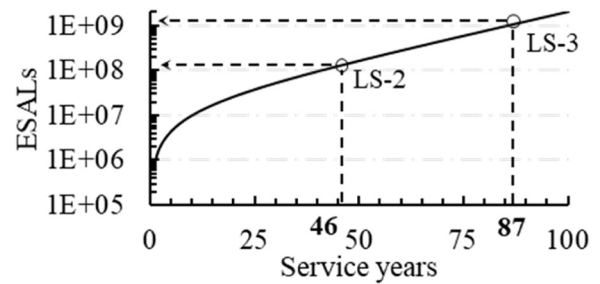


Fig. 10. Relationship between service years and equivalent single axle loads (ESALs).

the maximum applied load was 7 kN with end rotation  $\theta_{end} = \theta_{field} = 0.001$  rad, in the real-world application, many possible combinations of multiple ESALs could lead to the same end rotation [18, 24]. In order to simplify the calculation and to derive a conservative estimation of ESALs, the test load  $P_0 = 7$  kN was assumed to be equivalent to one standard 80 kN ESAL traveling on the bridge. Based on the fourth power rule [27,28] (Eq. 5), the corresponding LEFs were calculated and the applied fatigue cycles ( $N$ ) could be converted to ESAL.

$$\text{load equivalent factor}(LEF) = \left(\frac{P}{P_0}\right)^4 \quad (5)$$

$$ESAL = LEF \times N \quad (6)$$

In Eq. 5,  $P$  is the maximum applied load in the test while  $P_0$  was the assumed standard test load which represents one standard 80 kN ESAL on the field.  $N$  is the number of cycles in fatigue tests. The converted ESALs were summarised in Table 5. Based on the converted ESALs from the fatigue tests, the service life of LS-2 was estimated to be 46 years (Fig. 10) while the service life of LS-3 was estimated to be 87 years. For a conservative estimation, the minimum estimation from LS-2 was adopted so that the predicted service life was approximately equal to 46 years. Of course, this estimation was likely to be higher than the actual service life in real world application as it only considered the traffic and temperature effects while other effects such as corrosion of the reinforcement bars and abrasion of the slab surface were ignored. Nevertheless, according to the historical maintenance and pavement management records [14], a concrete link slab normally only had an expected service life of 20 years and required a major maintenance every 10 years. These results demonstrated another advantage of using hybrid-ECC for the construction of link slab as the longer service life might substantially reduce the maintenance cost of the connection.

##### 4.2. Development of midspan deflection

Fig. 11 shows the development of midspan deflection of LS-2 during the fatigue test. As shown in Fig. 11a, LS-2 survived the first ten million cycles Phase I test. During this phase the slab demonstrated a promising deformation control ability. In particular, the midspan deflection at upper load level (7 kN) only increased from 0.68 mm at the first cycle to 1.50 mm at the ten millionth cycle (Fig. 11a). It should be noted that

Table 5  
Calculation of ESALs from fatigue tests.

Test	$P_0$	$P$	$N$	LEF	ESALs	Total ESALs	Service years
LS2 (Phase I)	7	7	$1.0E+07$	1	$1.0E+07$	$1.4E+08$	46
LS2 (Phase II)		50.8	$4.5E+04$	2774	$1.1E+08$		
LS-3		33.6	$2.0E+06$	531	$1.1E+09$	$1.1E+09$	87

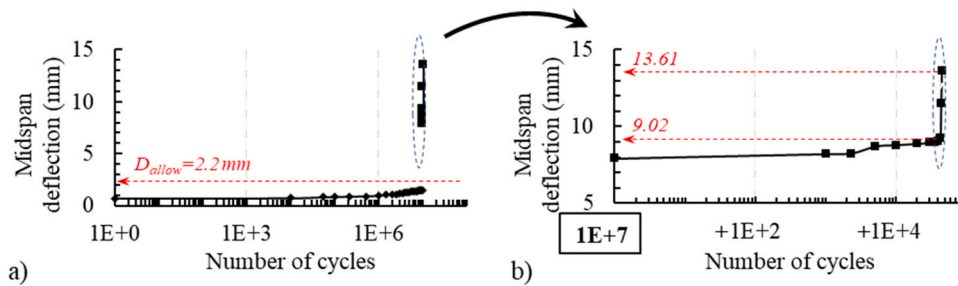


Fig. 11. Development of midspan deflection of LS-2. (a) Phase I and (b) Phase II.

even after ten million cycles, the maximum midspan deflection was still within the allowable midspan deflection limit of  $D_{allow} = 2.2$  mm, which is corresponding to an allowable end rotation  $\theta_{allow} = 0.00375$  rad at service limit state.

For the Phase II test, as shown in Fig. 11b, the midspan deflection increased to 9.02 mm after an additional of 43,000 cycles. Then the deformation further increased quickly to 13.61 mm at the 45,318th cycle when the slab was failed. Failure of LS-2 was caused by the fatigue failure of one of the reinforcement bars (on which gauge S1 was installed) within the link slab. Therefore, the specimen did not fail suddenly and the test was stopped when the deformation reached the safe deformation limit of the set up.

Fig. 12 shows the deflection hysteresis curves at some selected cycles for LS-2. The lower bound midspan deflection was increased from 0.28 mm at the first cycle to 1.15 mm at the ten millionth cycle in Phase I test. Hence, only a small plastic deformation of 0.87 mm was accumulated. Table 6 summarises the changes of the slab's stiffness  $k$  which is calculated by dividing the applied load range  $\Delta P$  (kN) with the corresponding deflection range  $\Delta d$  (mm). As shown in Table 6, the deflection range was slightly decreased from 0.40 mm at the first cycle to 0.36 mm at the ten millionth cycle. This led to a slight increase of  $k$  from 16.6 kN/mm to 17.5 kN/mm. Such result was reasonable since when more microcracks were formed within the ECC slabs as more fatigue cycles were applied, the reinforcement bars (which remained elastic in Phase I) would have gradually made more contribution and slightly increased the slab's stiffness. In Phase II test, as both the load level and range were much increased beyond normal service level and the reinforcement bars were yielded, stiffness degradation was observed so that the slab's stiffness was reduced from 9.8 kN/mm to 9.0 kN/mm and then 7.1 kN/mm during the 10,000th cycle, 43,000th cycle and 45,000th cycle of the Phase II test, respectively.

For LS-3, hysteresis curves of midspan deflection at some selected cycles are shown in Fig. 13 while the change of stiffness are again summarised in Table 6. Similar to LS-2, the slab's stiffness was increased from 10.7 kN/mm at the first cycle to 11.8 kN/mm at the one millionth cycle and then to 12.1 kN/mm at the two millionth cycle, respectively. Such a slight increase was again caused by the increase in stiffness contribution of the reinforcement bars as more microcracks were formed.

After two million cycles were applied on LS-3, it was unloaded and

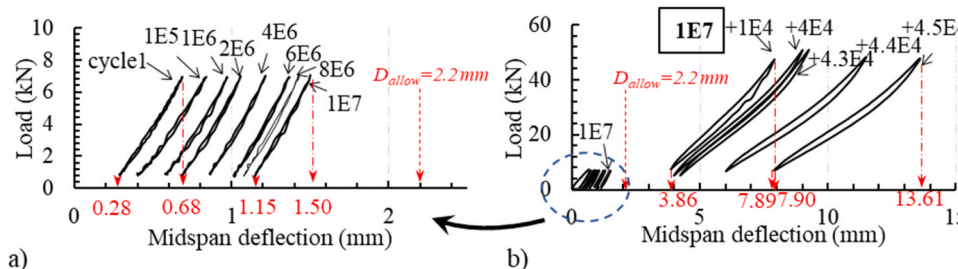


Fig. 12. Deformation hysteresis curves of LS-2 (a) Phase I and (b) Phase II.

Table 6  
Stiffness of the link slabs tested.

	Number of cycles	$d_{upper}$ (mm)	$d_{lower}$ (mm)	$\Delta d$ (mm)	$k$ (kN/mm)
LS-2	1	0.68	0.28	0.40	16.6
Phase I	5000000	1.31	0.95	0.36	17.4
loading	10000000	1.50	1.15	0.36	17.5
LS-2	1	7.90	3.86	4.05	9.8
Phase II	43000	9.27	4.22	5.05	9.0
loading	45000	13.61	7.89	5.72	7.1
LS-3	1	4.81	2.14	2.67	10.7
	1000000	6.14	3.62	2.52	11.8
	2000000	6.43	3.93	2.50	12.1

Legends:  $d_{upper}$ —midspan deformation at maximum load level,  $d_{lower}$ —midspan deformation at maximum load level,  $\Delta d = d_{upper} - d_{lower}$ ,  $k$  = stiffness of link slab

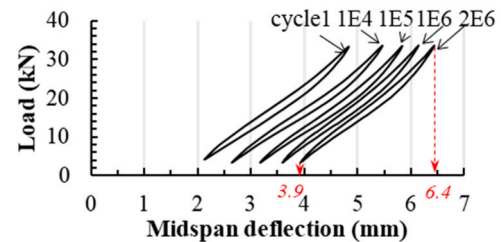


Fig. 13. Deformation hysteresis curves of LS-3.

an unrecoverable plastic midspan deformation of 3.71 mm was observed. Static test was then performed to obtain the residual static strength of the slab. Fig. 14 shows the load-midspan deformation curve obtained. Due to the unrecoverable plastic deformation, the curve starts with an offset deformation of 3.71 mm. The residual strength of the slabs was 67.7 kN at a midspan deflection of 16.11 mm. This residual strength of LS-3 was actually slightly higher than the ultimate strength of LS-1 (67.1 kN). Such a slight increase could be probably caused by the slight variation of the materials strength of the hybrid ECC as well as minor strength hardening of the reinforcement bars during the fatigue test (see Section 4.4 for more details). Hence, it can be concluded that LS-3 neither substantial degradation of stiffness nor decrease of ultimate

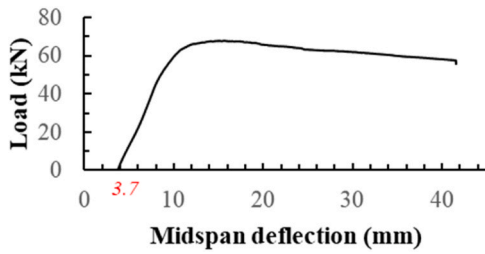


Fig. 14. Midspan deflection curve of residual static strength test of LS-3.

strength occurred despite after two million overload fatigue cycles.

### 4.3. Cracking behaviour

During Phase I test of LS-2, multiple microcracks were observed. As shown in Fig. 15a, no crack was visible after the first cycle. After five million load cycles, some microcracks were observed at the midspan section (Fig. 15b). As shown in Fig. 15c, after ten million load cycles, more microcracks were developed and extended from the midspan. Crack widths measured by DIC are shown in Fig. 16 which showed that LS-2 demonstrated very good crack width control ability in Phase I when the slab was under service loading. The maximum crack width recorded was approximately equal to 0.05 mm even after 10 million cycles which much less than the allowable serviceability limit of  $w_{limit} = 0.2$  mm. In Phase II test where a much higher load range of 5.1–50.8 kN was applied, more microcracks was developed along the debonding length as shown in Fig. 17. Similar cracking development patterns were observed at the 1st, 10,000th, and 40,000th cycles before the slab failed as shown in Figs. 17a, 17b and 17c, respectively. This demonstrated a stable development of the cracks before fatigue failure. During fatigue failure, microcracking were developed at the midspan area and a major crack with width larger than 0.5 mm was observed (Figs. 17d and 18). It was noted that the maximum crack width of LS-2 was still controlled within  $w_{limit} = 0.2$  mm within the first 40,000 cycles during the Phase II test (Figs. 17c and 18a) and the major crack was only formed at the last few thousand cycles (Figs. 17d and 18b) before failure occurred. Hence, it can be concluded even under an overload condition, LS-2 still

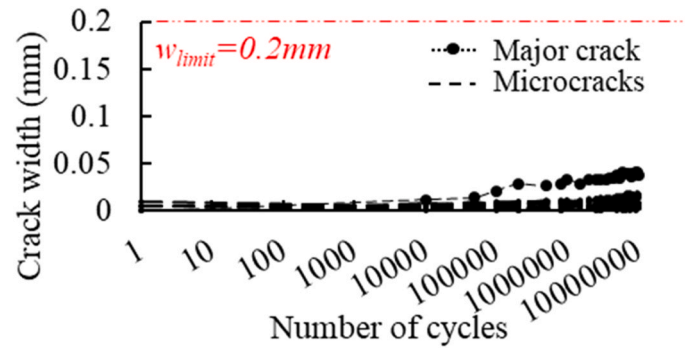


Fig. 16. Crack width development at Phase I test of LS-2.

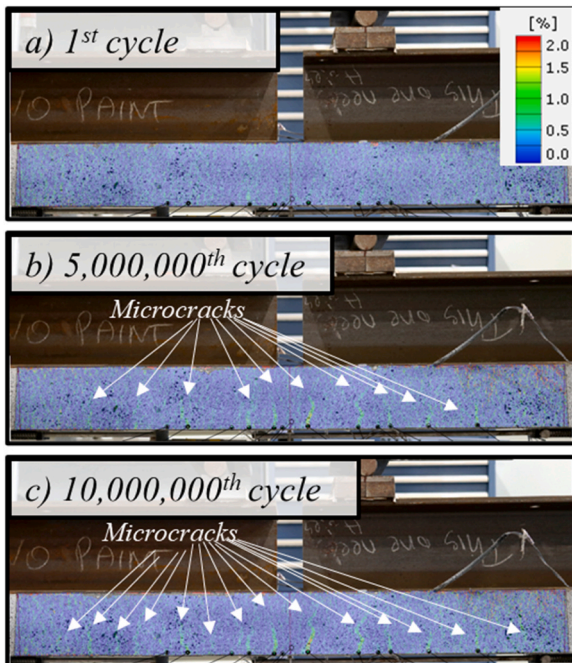


Fig. 15. Cracking behaviour during Phase I test of LS-2.

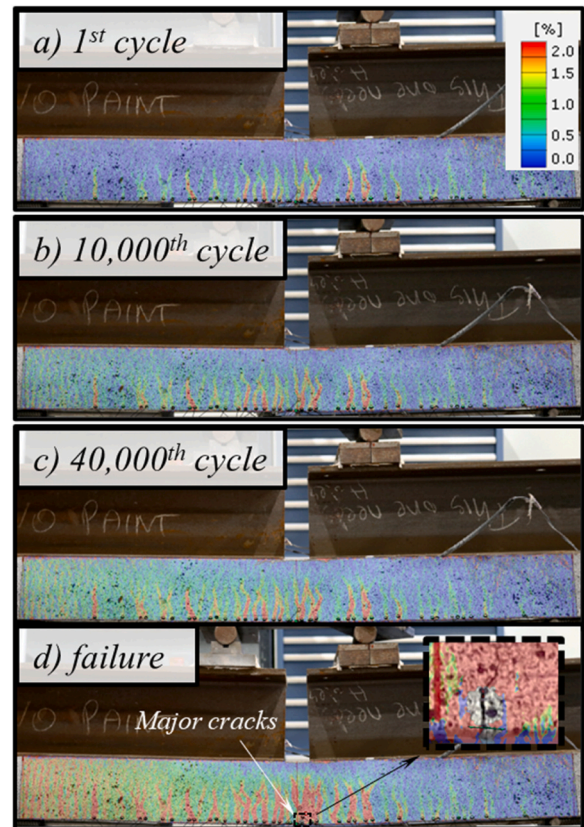


Fig. 17. Cracking behaviour during Phase II test of LS-2.

demonstrated a good crack width control ability before the fatigue failure occurred.

LS-3 was first tested under an overload load range and then followed by a static residual strength test. Fig. 19 shows the cracking patterns of LS-3 observed in the test. A few microcracks were invisible in the first cycle (Fig. 19a) due to the large load range. More cracks were then developed after one million (Fig. 19b) and two million cycles (Fig. 19c). As shown in Fig. 20, the maximum crack width observed was increased from 0.07 mm at the first cycle to 0.09 mm at the two millionth cycle which was still less than  $w_{limit} = 0.2$  mm. These results again demonstrated the advanced crack width control ability of the slab even under overload condition.

The cracking patterns observed during the static residual strength test were shown in Fig. 21. Fig. 21 shows that as the loading increased, more microcracks were developed. At the peak load, a major crack was formed as highlighted in red colour in Fig. 21c. As shown in Fig. 22, even when the peak load was reached with end rotation equal to 0.019 rad

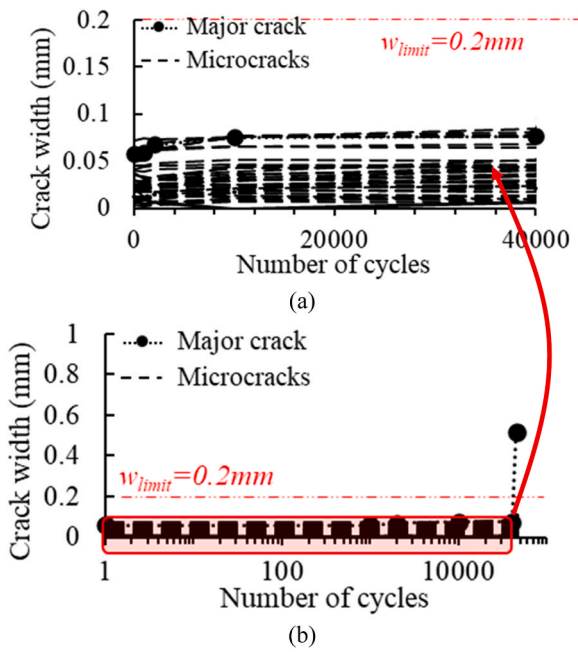


Fig. 18. Crack width development under Phase II fatigue loading on LS-2. (a) first 40,000 cycles, (b) up to fatigue failure after 45,000 cycles.

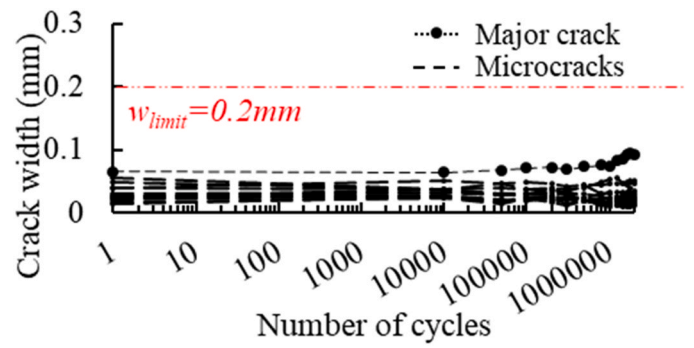


Fig. 20. Crack width development history of LS-3 under an overload scenario.

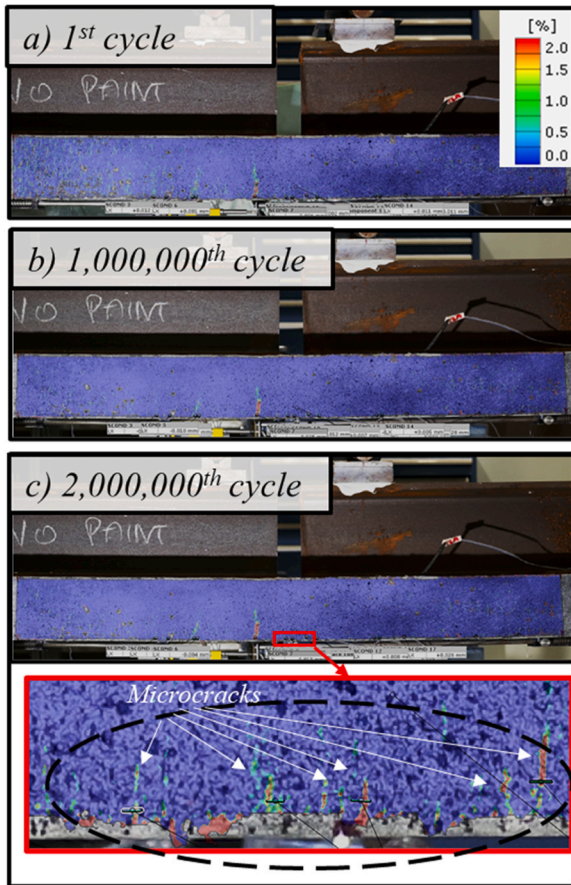


Fig. 19. Cracking behaviour of LS-3 under an overload scenario.

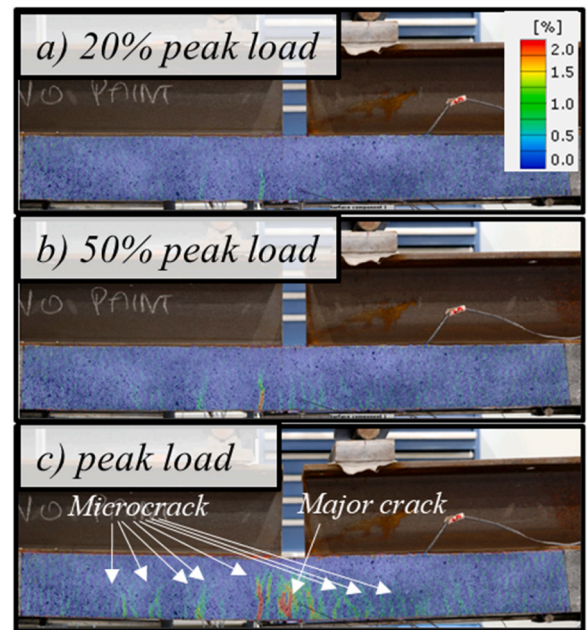


Fig. 21. Cracking behaviour of LS-3 during the static residual strength test.

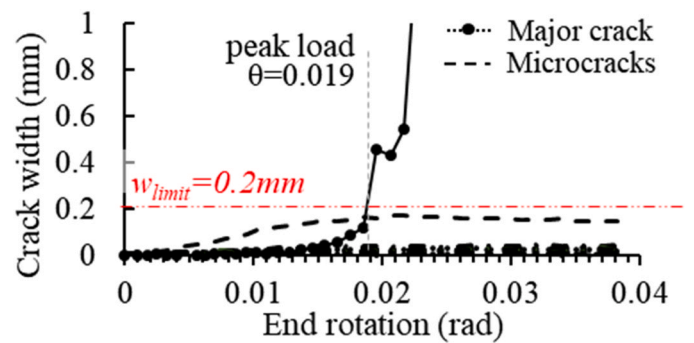


Fig. 22. Crack width development history of LS-3 during the static residual strength test.

(five time the allowable limit of 0.00375 rad), widths of all microcracks were well controlled within  $w_{limit} = 0.2$  mm. The width of the major crack was only increased after the peak load to 0.45 mm and then

exceeded 1 mm as the deformation increased. Therefore, for LS-3, the static residual strength test results shown that crack width control ability of the slab were not affected even after significant fatigue damage had been induced to the slab and only seriously affected after the ultimate residual strength was reached.

#### 4.4. Strain in reinforcement bars and ECC slabs

Tables 7 and 8 summarise the strains measured at some selection cycles in Phase I and Phase II tests of LS-2, respectively. In addition, Fig. 23a shows the maximum tensile strain ( $\epsilon_{max}$ ) measured at the midspan gauges S1 and S2 and S3 during Phase I test. Fig. 23a and Table 8 show that  $\epsilon_{max}$  was only slightly increased from the first cycle to after ten million cycles. Furthermore, all maximum strain values (248–301  $\mu\epsilon$ ) were much less than the elastic strain limit (2500  $\mu\epsilon$ ) of the reinforcement bars. In particular, the maximum strain attained (301  $\mu\epsilon$ ) at the end of the Phase I test after 10 million cycles was also much lower than the 40% yield strain service limited (i.e., 1000  $\mu\epsilon$ ) specified by the AASHTO design code [25]. However, during Phase II fatigue test, as shown in Fig. 23b and Table 8,  $\epsilon_{max}$  measured by gauges S1 and S2 were greater than the elastic limit due to the higher applied loads.

After Phase II test of LS-2 was completed, the ECC cover was removed. It was found that the reinforcement bar on which gauge S1 was installed showed significant amount of fatigue damaged (Fig. 24). The cross section of the reinforcement bar showed a typical fatigue damage pattern. This fatigue damage was also reflected in the strain development history shown in Fig. 23b. A sudden drop of S1 strain curve was noted between 40,000th - 44,000th cycle while strain measured by gauge S2 was increased due to stress redistribution.

It was noted that the strain along the reinforcement bars was redistributed as the fatigue cycle increased. As shown in Fig. 25, absolute slope of the curves increased from the first cycle to the ten millionth cycle. Meanwhile, the neutral section (i.e., where strain equals zero) of the reinforcement bars gradually moved towards the midspan section. This was expected as more stress was transferred from the ECC to the reinforcement bars at the midspan as more microcracks were formed.

In Phase I test of LS-2, the average tensile strain measured at the ECC slab surface by gauges C1, C2, and C3 was found to increase from 250  $\mu\epsilon$  at the first cycle to 475  $\mu\epsilon$  at the ten millionth cycle (Fig. 26a). In Phase II test, the maximum strain was increased to 9700  $\mu\epsilon$  which was recorded by gauge C2 at the 1,000th cycle. Note that readings from C3 were no longer available after 1000 cycles in Phase II test due to the failure of the gauge. Fig. 27 shows the strain distribution along the height of the ECC slab at the midspan section recorded by gauges C4, C5 and C6. Fig. 27 shows that from Phase I test to Phase II test, the neutral axis position of the slab gradually moved from approximately 30 mm to 60 mm measured from the slab bottom surface. This demonstrated the redistribution of the stress along the height of the ECC slab as the number of loading cycle increased. As cracks propagated along the height, it caused the neutral axis position to move upward.

For LS-3, the strain developed history of reinforcement bars were shown in Fig. 28. Table 9 summarises the strains measured at the one millionth and two millionth cycles. A maximum tensile strain of 2770  $\mu\epsilon$  was recorded by gauge S3 at the two millionth cycle. It was slightly higher than the elastic limit (2500  $\mu\epsilon$ ) while strains from S1 and S2 were still within the elastic limit. This result shown that while LS-3 was tested under an overload condition, two out of the three reinforcement bars were still not yielded at the end of the fatigue test after two million

cycles.

During the fatigue tests, accumulated plastic strains was observed in reinforcement bars for both LS-2 and LS-3. As different sections of the reinforcement bars were subjected to different stress levels, different accumulated plastic strains were measured at different sections. The last row of Tables 7–9 listed the accumulated plastic strains ( $\epsilon_{pl}$ ) at different load cycles measured at different sections by gauges S1 to S6. Values of  $\epsilon_{pl}$  shown in Tables 7–9 were calculated by subtracting the elastic strain from the total strain measured at the lower load level. The results shows that the development of  $\epsilon_{pl}$  was generally related to the maximum applied strain range  $\epsilon_{max}$  as well as the section location. From Tables 7–9, it can be clearly seen that higher plastic strain was developed at the midspan section (i.e., at gauges S1 to S3) and increased as  $\epsilon_{max}$  was increased. For the Phase I test of LS-2, since both the maximum load and the load range applied were small, only a small amount of plastic strain was developed and values of  $\epsilon_{pl}$  did not change significantly between the five millionth and ten millionth cycles (Table 7). For the Phase II test of LS-2 and LS-3, since a higher maximum load and load range were applied, higher plastic strains were recorded. However, from Tables 8 and 9 the maximum plastic strain was still lower than the yield strain of the reinforcement bars.

#### 5. Comparison of hybrid-ECC link slabs performance with concrete and monofibre ECC link slabs

In order to compare of the fatigue performance of the hybrid ECC link slabs tested in this study with other link slabs fabricated with concrete and different monofibre (PE or PVA) ECC materials, results reported in the literature from three different previous studies [11,16,29] are retrieved from the corresponding publication compared with the current study results. It should be noted that in order to provide a reasonable and fair comparison, specimens studies in [11,16,29] were prepared by using a similar setup, a same debonding length ratio of 5% and a similar reinforcement bar ratio (between 1% and 1.13%). Summary of these tests and the link slabs' performances under static tests are given in Table 10. It should be noted that these tested specimens were prepared with different sizes and span lengths. Furthermore, it should also be noted that all these three previous studies involved one or two link slabs for static tests and two to three link slabs for fatigue test which is similar to the number of link slabs test in this study. The material properties of ECC and concrete used in the link slabs tested in those studies are summarised in Table 11.

Under the static tests, as listed in Table 10, the ultimate deflection to span ratio was used as an indicator for the link slab's ductility comparison. It was found that the deflection to span ratio of link slabs at the peak load  $P_u$  are in a sequence of PL-2 (static) (PE-ECC; ratio=1/49, [11]) > LS-1 (hybrid-ECC; ratio=1/60, this study) > L0N (PVA-ECC; ratio=1/74, [16]) > LS-ECC-Control (PVA-ECC; ratio=1/107, [29]). Hence, the deflection to span ratio of the link slabs tested in this study is smaller than all other slabs except the one tested in [29] which showed a slightly smaller ratio (1:49 vs 1:60). However, it should be noted that for the slab tested in [29], the PE-ECC used was designed to have a very high

**Table 7**

Reinforcement bars strains measured at five millionth and ten millionth cycles during Phase I test of LS-2.

Cycle	5000,000						10,000,000					
	S1	S2	S3*	S4	S5	S6	S1	S2	S3 *	S4	S5	S6
$\epsilon_{min}$	181	220	/	72	-14	-125	161	223	/	35	-66	-206
$\epsilon_{max}$	265	290	/	115	3	-116	248	301	/	72	-49	-203
$\Delta\epsilon$	84	70	/	43	17	9	87	78	/	37	17	3
$\epsilon_{mean}$	223	255	/	94	-6	-121	205	262	/	54	-58	-205
$\epsilon_{pl}$	160	197	/	66	-17	-116	140	200	/	29	-69	-197

Note: All strain values are  $\mu\epsilon$ . Tensile strain is positive.

\*Gauge S3 failed to record any data after approximately two million cycles in Phase I test.

$\epsilon_{min}$ ,  $\epsilon_{max}$ ,  $\epsilon_{mean}$  and  $\epsilon_{pl}$  are the minimum, maximum, average and plastic strain, respectively.

$\Delta\epsilon = \epsilon_{max} - \epsilon_{min}$ . and  $\epsilon_{mean} = (\epsilon_{max} + \epsilon_{min})/2$

**Table 8**  
Reinforcement bars strains measured at 20,000th and 40,000th cycles during Phase II test of LS-2.

Cycle	20,000						40,000					
	S1	S2	S3 *	S4	S5	S6	S1^	S2	S3 *	S4	S5	S6
$\epsilon_{min}$	1204	1115	/	720	69	-228	/	1193	/	925	104	-242
$\epsilon_{max}$	3359	2792	/	1666	205	-277	/	2900	/	1927	231	-274
$\Delta\epsilon$	2155	1677	/	946	136	-49	/	1707	/	1002	127	-32
$\epsilon_{mean}$	2282	1954	/	1193	137	-253	/	2047	/	1426	168	-258
$\epsilon_{pl}$	1120	1023	/	677	53	-223	/	1101	/	882	88	-237

Note: All strain values are  $\mu\epsilon$ . Tensile strain is positive. Strain higher than yield strain are underlined.

\*Gauge S3 failed to record any data after approximately two million cycles in Phase I test.

^Gauge S1 failed to record any data after approximately 40000 cycles in Phase II test.

$\epsilon_{min}$ ,  $\epsilon_{max}$ ,  $\epsilon_{mean}$  and  $\epsilon_{pl}$  are the minimum, maximum, average and plastic strain, respectively.

$\Delta\epsilon = \epsilon_{max} - \epsilon_{min}$ . and  $\epsilon_{mean} = (\epsilon_{max} + \epsilon_{min})/2$

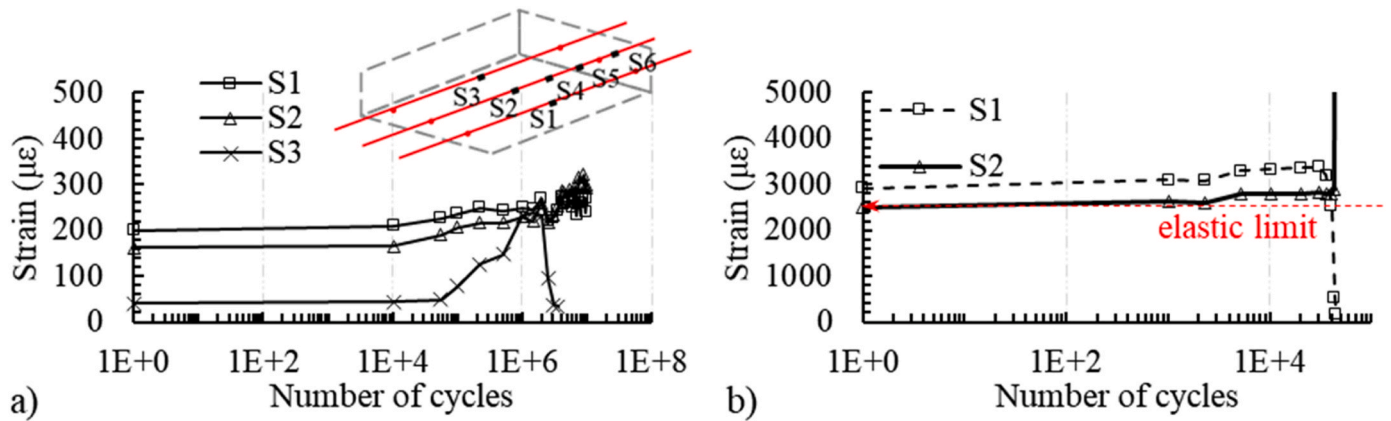


Fig. 23. Reinforcement bars strains measured for LS-2 (a) Phase I test, (b) Phase II test.

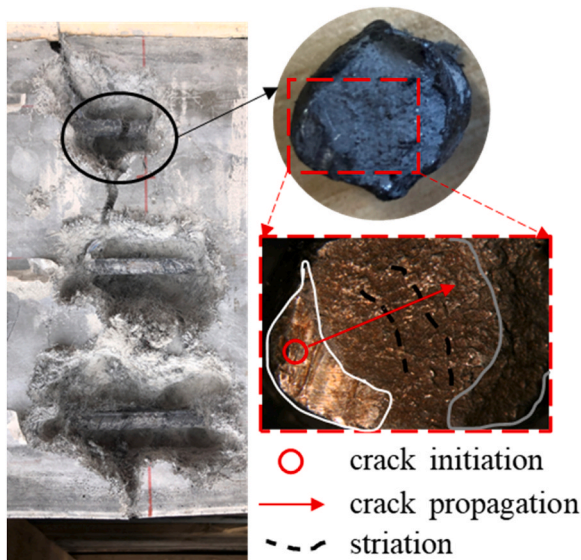


Fig. 24. Fatigue damage of reinforcement bar for LS-2.

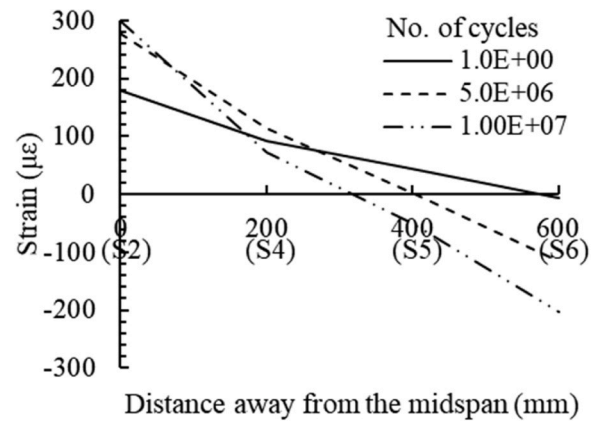


Fig. 25. Strain distributions along reinforcement bars at different load cycles during Phase I fatigue test of LS-2.

tensile strain capacity (7% vs 2.7% of the hybrid ECC used in this study) which could be more costly to produced. In addition, its width was 500 mm which is 167% of the slab width (300 mm) tested in this study. In terms of end rotation, the last column in Table 10 showed the higher ductility of the hybrid-ECC link slab compared with PVA-ECC link slabs.

For the fatigue testing, the test details are summarized in Table 12. It should be noted that the total number of fatigue loading cycles applied in all these three studies [11,16,29] is equal to 5.3 million which was only about half of the cycles applied in the LS-1 Phase I test in this study.

Table 12 also shows the results under different fatigue loading range levels  $\Delta P$  which is expressed as percentage of the ultimate static load  $P_u$ . It should also be noted that in these three previous studies [11,16,29], the loading range applied were ranging from 20% to 58%.

Table 12 clearly shows that the hybrid ECC link slabs tested in this study and those monofibre from [11,16,29] outperformed the concrete link slab PL-1 (concrete) [11]. Despite a lower fatigue loading applied, the concrete link failed in less than 650 thousand cycles and resulted in the largest deflection ratio among tested slabs.

From Table 12, it can be seen that the hybrid-ECC link slabs tested generally showed a better fatigue performance when compared with other monofibre ECC link slabs. For example, for hybrid-ECC link slab LS-3 tested with  $\Delta P = 45\%$  after two million cycles, no significant

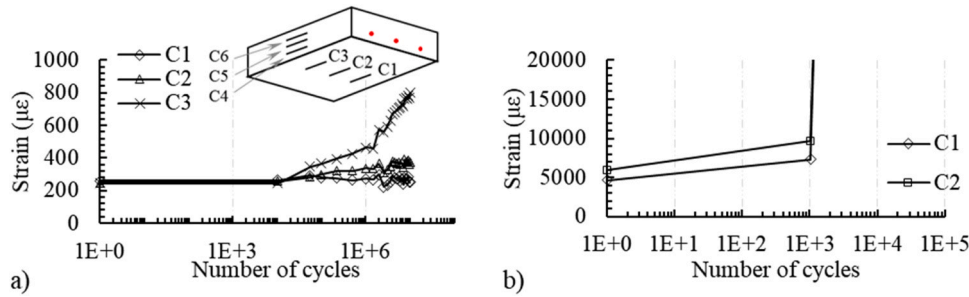


Fig. 26. ECC slabs surface strains measured for LS-2. (a) Phase I test and (b) Phase II test.

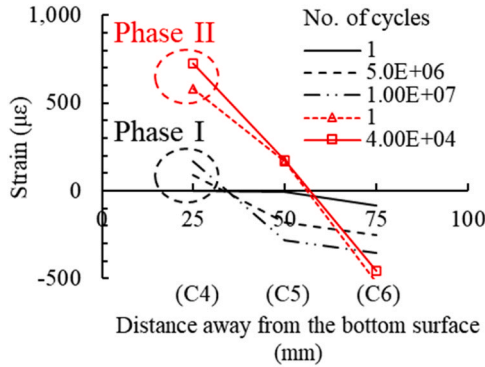


Fig. 27. Strain distribution along the height of ECC slab of LS-2 at different load cycles.

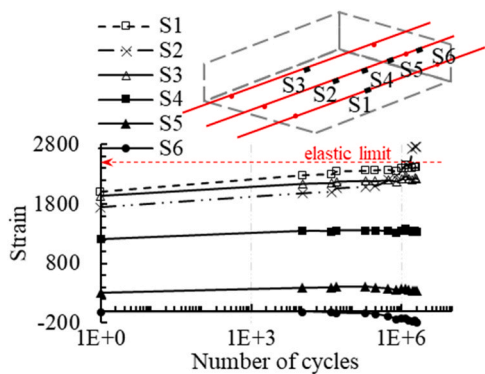


Fig. 28. Reinforcement bars strains measured for LS-3 during fatigue loading.

damage or performance degradation were observed and the crack width was still < 0.1 mm. The stiffness ( $k = \Delta P / \Delta d$ , where  $\Delta d$  is the corresponding deflection increment) at the first cycle ( $k = 10.7$ ) was similar (actually slightly smaller than) the stiffness at the ultimate cycle ( $k = 12.1$ ). In contrast, all other PVA-ECC link slabs showed a reduction

Table 9  
Reinforcement bars strains measured at the one and two millionth cycles of LS-3.

Cycle	1000,000						2000,000					
	S1	S2	S3	S4	S5	S6	S1	S2	S3	S4	S5	S6
$\epsilon_{min}$	1139	1272	1352	801	275	-102	1150	1272	1765	798	240	-168
$\epsilon_{max}$	2228	2391	2365	1354	379	-119	2228	2408	<u>2770</u>	1333	336	-191
$\Delta \epsilon$	1089	1119	1013	553	104	-18	1078	1136	1005	535	96	-23
$\epsilon_{mean}$	1683	1831	1858	1078	327	-110	1689	1840	2267	1066	288	-180
$\epsilon_{pl}$	1066	1194	1266	755	264	-99	1077	1194	1679	752	229	-165

Note: All strain values are  $\mu\epsilon$ . Tensile strain is positive. Strain higher than yield strain are underlined.

$\epsilon_{min}$ ,  $\epsilon_{max}$ ,  $\epsilon_{mean}$  and  $\epsilon_{pl}$  are the minimum, maximum, average and plastic strain, respectively.

$\Delta \epsilon = \epsilon_{max} - \epsilon_{min}$ . and  $\epsilon_{mean} = (\epsilon_{max} + \epsilon_{min}) / 2$

of stiffness after sustained a lower load level ( $\Delta P = 20\%$ ) with less fatigue cycles (<1000,000) [16,29] but results in a higher crack width (0.1–0.4 mm).

When compared with the PE-ECC link slabs studied in [11], Table 12 show that even though the hybrid-ECC link slab LS-2 (Phase II) was loaded at a higher fatigue load level of  $\Delta P = 68\%$  than the  $\Delta P = 58\%$  subjected by the PE-ECC link slab PL-2 (Phase II), they both practically achieved the same similar fatigue life (45,318 cycles vs 69500 cycles) while the hybrid-ECC link slab LS-2 (Phase II) showed a slightly smaller deflection to span ratio (1/94 vs 1/91) [11]. This is expected as PE-ECC has lower ultimate strength and modulus (Table 11) which led to less deformation control ability under fatigue loading. Meanwhile, smaller steel reinforcement bars strain was observed in the hybrid-ECC link slab LS-2 at both the first (2513  $\mu\epsilon$  vs 2770  $\mu\epsilon$ ) and last cycles (2900  $\mu\epsilon$  vs 5395  $\mu\epsilon$ ) despite the same reinforcement ratio (1.13%, Table 10) was used but a higher fatigue load ratio was applied. This implied that during the fatigue testing, the hybrid ECC actually took up more loading than the PE-ECC. Hence, although PE-ECC had a high strain capacity that increased the ductility of the link slab under static loading (Table 10), its low modulus actually weakened the fatigue performance. The hybrid-ECC used in this study demonstrated a better balanced stiffness and strain capacity, which showed better static and fatigue performance for link slab application.

## 6. Conclusions

This experimental study investigated the behaviours of three hybrid-ECC link slabs (LS-1, LS-2 and LS-3) under static and fatigue loadings. For the best knowledge of the authors, for first time, a fatigue test was conducted on hybrid ECC link slabs with up to ten million fatigue loading cycles. The ultimate flexural strength, deformability, crack width control ability, and estimated service life were investigated. Based on the test results, the following important conclusions can be drawn.

1. The static loading test on the first link slab LS-1 demonstrated that the hybrid-ECC link slab has high deformability and crack width control ability. The ultimate load was achieved at a midspan deflection to span ratio of 1/60. At the peak load, the maximum

**Table 10**  
Summary of test setup of link slabs and their performance under static loading.

	Material (fibres used)	Size of debonded slab / mm <sup>3</sup> Length×Width×Depth	Static test ID	Fatigue test ID	span length / mm	Reinforcement ratio (%)	Static test results at peak load $P_u$		
							Peak load $P_u$ / kN	Deflection / mm (ratio to span)	End rotation / rad
This study	hybrid-ECC (PE and ST)	875 × 300 × 100	LS-1	LS-2 (Phases I and II), LS-3	1275	1.13	67.1	21.1(1/60)	0.035
[11]	Concrete	1550 × 500 × 100	PL-1 (static)	PL-1	2550	1.13	^	^	^
[29]	ECC (PE)	1550 × 500 × 100	PL-2 (static)	PL-2	2550	1.13	43.18	52.15(1/49)	^
	ECC (PVA)	330 × 176 × 60	LS-ECC- Control	LS-ECC-40, LS-ECC-55	810	1.1	12.16	7.59(1/107)	0.0205
[16]	ECC (PVA)	330 × 176 × 60	LON	L4L, L5L, L4H	810	1.0	10.41	11(1/74)	0.0289

^ indicates that no data was given in the corresponding publication.

**Table 11**

Properties of materials used in tested link slabs used in study and other previous similar studies.

	This work	[11]		[29]	[16]
Material (fibres used)	hybrid-ECC (PE and ST)	ECC (PE)	Concrete	ECC (PVA)	ECC (PVA)
Young's Modulus (GPa)	28.3	15.2	29	^	^
Tensile strength (MPa)	7.3	4.67	^	^	^
Strain at tensile strength (%)	2.7	7	^	^	^
Compressive strength (MPa)	94.5	36.5	28.1	55.5	67

^ indicates that no data was given in the corresponding publication.

- crack width was controlled within the 0.2 mm allowable limit for application in an aggressive environmental condition.
- The hybrid-ECC link slabs demonstrated improved performance against the fatigue load under service and overload scenarios. The second link slab LS-2 survived 10 million cycles of fatigue loading ranging from 0.7 to 7.0 kN which was corresponded to a typical service loading scenario. After ten million cycles, the maximum midspan deflection of 1.5 mm under 7.0 kN loading was observed which was less than the serviceability limit of 2.2 mm. Multiple microcracks were developed while their crack widths were controlled within 0.1 mm. The test results demonstrated the promising fatigue performance of the hybrid-ECC link slab under service loading. After ten million cycles of service loading, LS-2 was subjected to a much higher load range of 5.1–50.8 kN which generated an end rotation equal to three times of the serviceability limit. Under this larger loading range, the slab failed after a further 45,000 cycles due the formation of a 1 mm wide crack and fatigue failure of one of the reinforcement bars.
  - The last link slab LS-3 survived two million cycles of fatigue loading ranging from 3.4 kN to 33.6 kN which corresponded to an overload scenario. The maximum crack width observed was still less than 0.2 mm at the end of two million cycles. The slab showed neither degradation in the overall stiffness nor ultimate flexural strength. This demonstrated the superior fatigue resistance of the slab under an overload scenario.
  - Fatigue test results obtained from LS-2 and LS-3 showed that the maximum strains developed in reinforcement steel bars were generally less than the yield limit for both the service and overload scenarios. The only exception was strain at midspan when LS-2 was subjected to very high stress range. However, due to the huge number of loading cycles applied, accumulated plastic strain was observed in all reinforcement bars at the end of fatigue tests.
  - Based on the fatigue test results which mainly considering traffic loading and temperature variation effect, the service life of the slabs was estimated to be more than 40 years. While this was likely to be an upper bound estimation, it doubled the normal service life of concrete link slabs. Hence, this study demonstrated that the hybrid ECC used has a high potential to be used in the future design of link slabs to improve fatigue performance and extend the service life in bridge construction. A preliminary comparison with test results obtained from the literature showed that the hybrid-ECC link slab demonstrated improved fatigue performances over concrete, PE-ECC, and PVA-ECC link slabs in a similar test setup.

Finally, one future potential research topic is to investigate the effect of different design parameters (e.g., the use of hybrid ECC with different compressive and tensile properties and steel reinforcement bars of different grades, the use of different reinforcement bar ratio and different loading types, and different support conditions etc.) on the fatigue flexural behaviour of the link slabs. Obviously, it is virtually

**Table 12**  
Structural performance of tested link slabs at fatigue loads.

Fatigue test ID	$P_{max}$ kN	$P_{min}$ kN	$\Delta P$ (ratio to $P_u$ )	Fatigue cycles	At the first cycle			At the last cycle				
					Midspace deflection, mm (ratio to span)	Strain of the steel bar, $\mu\epsilon$	Stiffness, $k = \Delta P / \Delta d$	Midspace deflection, mm (ratio to span)	Strain of the steel bar, $\mu\epsilon$	Stiffness, $k = \Delta P / \Delta d$		
This study	LS-2 (Phase I)	0.7	7.1	6.4 (10%)	10,000,000	0.68(1/1875)	162	16.6	1.5(1/850)	301	17.5	< 0.05
	LS-2 (Phase II)	5.1	50.8	45.7 (68%)	45,318	7.9(1/161)	2513	9.8	13.61(1/94)	2900	7.1	< 0.1
	LS-3	3.4	33.6	30.2 (45%)	2000,000	4.81(1/265)	1998	10.7	6.43(1/198)	2408	12.1	< 0.1
[11]	PL-1 (concrete)	1.43	14.3	12.87 (-)	630,600	7.62(1/335)	920	*	35.38(1/72)	*	*	*
	PL-2 (PE, Phase I)	1.43	14.3	12.87 (30%)	2000,000	8.62(1/296)	1514	*	12.18(1/209)	1900	*	*
	PL-2 (PE, Phase II)	2.8	28	25.2 (58%)	69,500	17.59(1/145)	2770	*	28.02(1/91)	5395	*	*
[29]	LS-ECC-40 (PVA)	3.65	6.08	2.43 (20%)	400,000	2.31(1/350)	1600	*	4.7(1/172)	1800	*	0.1
	LS-ECC-55 (PVA)	5.47	7.90	2.43 (20%)	400,000	3.61(1/224)	1800	*	5.4(1/150)	2100	*	0.15
[16]	L4L (PVA)	3.12	5.21	2.08 (20%)	400,000	2.75 (1/295)	1358	1.46	3.72 (1/218)	1664	1.04	0.15
	L5L (PVA)	4.68	6.77	2.08 (20%)	400,000	3.27 (1/248)	1562	1.68	4.67 (1/173)	2034	1.09	0.15
	L4H (PVA)	3.12	5.21	2.08 (20%)	1000,000	2.25(1/360)	1173	1.78	3.7(1/219)	1864	0.99	0.4

\* indicates that no data was given in the corresponding publication.

impossible to conduct such a comprehensive study experimentally due to the very high cost and time needed to conduct the fatigue tests. Towards this end, development of a numerical (finite element) model for predicting the fatigue performance of the link slab under various fatigue load levels will be an indispensable tool while the test results obtained in this study could provide some valuable data for the validation of such model. The validated model can then be used to conduct a comprehensive numerical parametric study to obtain more insights on the influence of different key design parameters on the performance of the slabs.

#### CRedit authorship contribution statement

**Shiyao Zhu:** Methodology, Software, Validation, Formal analysis, Investigation, Writing – original draft, Visualization. **C. K. Lee:** Conceptualization, Methodology, Investigation, Resources, Writing – review & editing, Supervision. **Y. X. Zhang:** Methodology, Writing – review & editing, Supervision.

#### Declaration of Competing Interest

The authors declare that they have no known competing financial interests or personal relationships that could have appeared to influence the work reported in this paper.

#### Data availability

Data will be made available on request.

#### Acknowledgement

UNSW Canberra's support for the first author to conduct this research received through TFS Scholarship are gratefully acknowledged.

#### References

- [1] Li VC. Introduction to Engineered Cementitious Composites (ECC). Engineered Cementitious Composites (ECC). Berlin, Heidelberg: Springer; 2019.
- [2] Ranade R, Li VC, Stults MD, Heard WF, Rushing TS. Composite Properties of High-Strength, High-Ductility Concrete. *Acids Mater J* 2013;110:413–22.
- [3] Kim MJ, Kim S, Yoo DY. Hybrid effect of twisted steel and polyethylene fibers on the tensile performance of ultra-high-performance cementitious composites. *Polymers* 2018;10:879.
- [4] Zhou Y, Xi B, Yu K, Sui L, Xing F. Mechanical properties of hybrid ultra-high performance engineered cementitious composites incorporating steel and polyethylene fibers. *Materials* 2018;11:1448.
- [5] Yu QQ, Yu JT, Dai JG, Lu ZD, Shah SP. Development of ultra-high performance engineered cementitious composites using polyethylene (PE) Fibers. *Constr Build Mater* 2018;158:217–27.
- [6] Zhu S, Zhang YX, Lee CK. Polyethylene-Steel Fibre Engineered Cementitious Composites for Bridge Link Slab Application. *Structures* 2021;32:1763–76.
- [7] Barth KE, Michaelson GK, Tenssny RM, Woldegabriel B. Experimental assessment of link slabs in continuous span applications of press-brake-formed tub girders. *Bridge Struct* 2022;18:65–74.
- [8] Caner A, Zia P. Behavior and Design of Link Slabs for Jointless Bridge Decks. *PCI J* 1998;43:68.
- [9] VicRoads. Cracks in Concrete. Technical Note TN 038: VicRoads; 2010.
- [10] Kim YY, Fischer G, Li VC. Performance of bridge deck link slabs designed with ductile engineered cementitious composite. *Struct J* 2004;101.
- [11] Hou MJ, Hu KX, Yu JT, Dong SW, Xu SL. Experimental study on ultra-high ductility cementitious composites applied to link slabs for jointless bridge decks. *Compos Struct* 2018;204:167–77.
- [12] Hong Y. Analysis and Design of Link Slabs in Jointless Bridges with Fibre-Reinforced Concrete. *UWSpace*; 2014.
- [13] Ulku E, Attanayake U, Aktan H. Jointless Bridge Deck with Link Slabs: design for Durability. *Transp Res Rec* 2009;2131:68–78.
- [14] Qian SZ, Li VC, Zhang H, Keoleian GA. Life cycle analysis of pavement overlays made with engineered cementitious composites. *Cem Concr Compos* 2013;35: 78–88.
- [15] Au A, Lam C, Au J, Tharmabala B. Eliminating deck joints using debonded link slabs: research and field tests in Ontario. *J Bridge Eng* 2013;18:768–78.
- [16] Chu K, Hossain KMA, Lachemi M. Static and Fatigue Behaviour of ECC link slabs in reinforced concrete girder joint-free bridges. *Structures* 2022;41:1301–10.
- [17] Zheng Y, Zhang LF, Xia LP. Investigation of the behaviour of flexible and ductile ECC link slab reinforced with FRP. *Constr Build Mater* 2018;166:694–711.

- [18] Lepech MD, Li VC. Application of ECC for bridge deck link slabs. *Mater Struct* 2009;42:1185.
- [19] El-SAFY A.K. Behavior of Jointless Bridge Decks: North Carolina State University; 1994.
- [20] State of Queensland Department of Transport and Main Roads. Drafting and Design Presentation Standards Manual. Volume 3, Structural drafting standards. Brisbane, Queensland: Queensland Department of Transport and Main Roads Library Services; 2018.
- [21] ASTM C39M-18. Standard Test Method for Compressive Strength of Cylindrical Concrete Specimens, ASTM International, West Conshohocken, Pa, 2018, ([www.Astm.org](http://www.Astm.org)).
- [22] Meng D, Huang T, Zhang YX, Lee CK. Mechanical behaviour of a polyvinyl alcohol fibre reinforced engineered cementitious composite (PVA-ECC) using local ingredients. *Constr Build Mater* 2017;141:259–70.
- [23] ASTM C1273–18. Standard Test Method for Tensile Strength of Monolithic Advanced Ceramics at Ambient Temperatures, ASTM International, West Conshohocken, Pa, 2018, [www.Astm.Org](http://www.Astm.Org).
- [24] Wing Kenneth M, Kowalsky Mervyn J. Behavior, analysis, and design of an instrumented link slab bridge. *J Bridge Eng* 2005;10:331–44.
- [25] American Association of State Highway and Transportation Officials, AASHTO LRFD Bridge Design Specifications, AASHTO, 2012.
- [26] Department of Infrastructure, Planning and Logistics in conjunction with Territory Traffic Surveys. Annual Traffic Report 2021. 2021.
- [27] Nilsson J-E, Svensson K, Haraldsson M. Estimating the marginal costs of road wear. *Transp Res Part A: Policy Pract* 2020;139:455–71.
- [28] Kinder D.F., Lay M. Review of the Fourth Power Law. Australian Road Research Board; 1988.
- [29] Hossain K.M.A., Ghatrehsamani S., Anwar M.S. Flexural fatigue performance of ECC link slabs for bridge deck applications. in Sustainable Bridge Structures: Proceedings of the 8th New York City Bridge Conference, ed. Mahmoud, K., CRC Press/Balkema, 2015; 247–260.